Feasibility of an MSE system on the TCV tokamak

M.R. Siegrist, N. Hawkes*, H. Weisen

Centre de Recherches en Physique des Plasmas
Association Euratom - Confédération Suisse
Ecole Polytechnique Fédérale de Lausanne
CH-1015 Lausanne, Switzerland

***Euratom/UKAEA Association**
Culham Science Centre
Abingdon, Oxfordshire, OX14 3DB, U.K.

Abstract

This paper presents a feasibility study for a MSE diagnostic on the TCV tokamak. A numerical simulation code has been used to identify the optimal port arrangement and geometrical layout. It predicts the expected measurement accuracy for a range of typical plasma scenarios. With the existing Neutral Particle Injector and a detection system based on current day technology, it should be possible to determine the safety factor with an accuracy of the order of 5%. A vertically injected beam through the plasma center would allow to measure plasmas which are centered above the midplane, a common occurrence in connection with ECRH/ECCD experiments. In this case a new and ideally more powerful NBI would be required.

Feasibility of an MSE system on the TCV tokamak

M.R. Siegrist, N. Hawkes, H. Weisen

1.0 Introduction

Since the first demonstration of a motional Stark effect (MSE) measurement on the Princeton PBX-M machine [1], this type of diagnostic has been installed on several machines [2,3,4,5] and is now recognized to be the main method to determine the magnetic pitch angle from which the poloidal field and the q-profile can be derived. The diagnostic relies on the availability of a sufficiently powerful neutral beam injector, apart from the nowadays standard sensitive detection system to determine the polarization.

It has been recognized long ago that this equipment can also be used to determine the plasma radial electric field and first attempts to do so have been reported, albeit with a yet rather poor signal-to-noise ratio [6].

The scientific program of the TCV tokamak could greatly profit from both a q-profile measurement as well as a determination of the radial electric field associated with a transport barrier. There are basically two main features which make TCV unique in its category: the coil system and vacuum vessel which allow to produce plasma cross sections with very flexible shapes and the powerful ECRH and ECCD system. The former renders profile reconstruction more challenging than usual and the constraints imposed by MSE data could greatly improve the reliability of the procedure. From the latter the interpretation of barrier formation in ECRH heated plasmas would certainly benefit.

Budgetary limitations and the fact that a NBI system (albeit of limited power) is already available on TCV were the main reasons for the decision to perform a detailed feasibility study for a MSE diagnostic on TCV. A numerical code developed at JET [7] allowed us to investigate the effect of different geometries and plasma and equipment parameters on the expected precision of such a measurement.

2.0 Possible geometries on TCV

The existing neutral particle injector (NPI) on TCV is mounted horizontally and emits particles in the midplane of the machine, in roughly radial direction. It can be turned in the midplane by about 11^{o} in either direction. For larger angles it is no longer possible to inject the whole beam diameter through the port arrangement. The combination of radial beam with the basically toroidal direction of the main magnetic field results in a vertical electric Lorentz field. For maximum detection sensitivity the lines of sight (LOS) should therefore be in a horizontal plane. The Doppler shift which separates the observed spectral

lines from the unshifted H_α line emitted mainly from the plasma edge is largest for radial LOSs. However, this results in a complete loss of spatial resolution, which would be optimum with a tangential LOS arrangement. Hence a compromise has to be found for these two conflicting requirements.

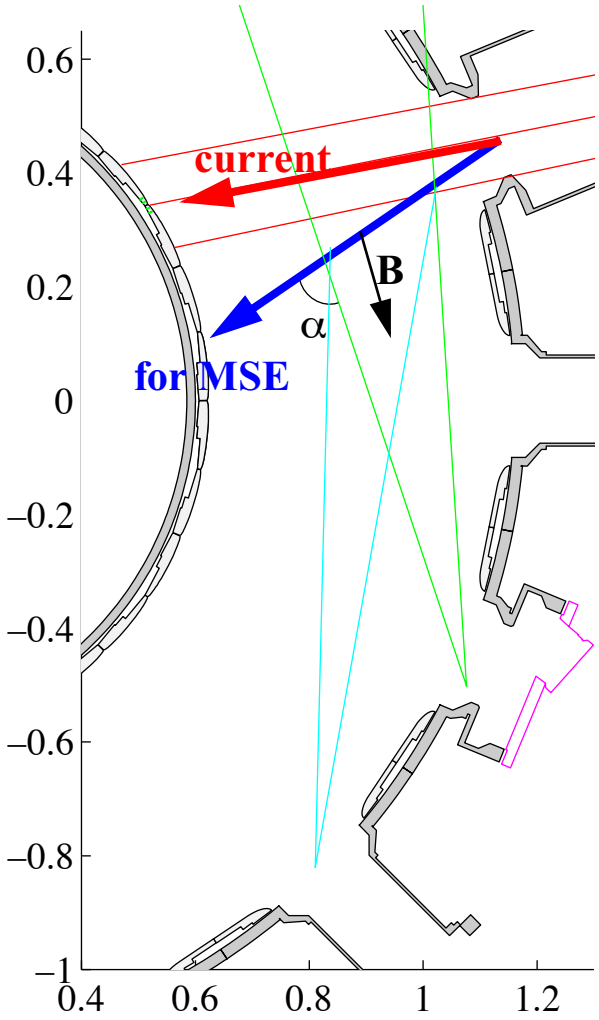

FIGURE 1. Port arrangement in the midplane with NPI and possible diagnostic ports

In toroidal direction the ports in the midplane of TCV are separated by an angle of 22.5^o and with the injector left in its current position the detection system could be placed in a neighboring port or either 2 or 3 ports away, hence forming angles of 22.5^o, 45^o and 67.5^o respectively with the injector port. With some re-arrangement of other diagnostics, ports above or below the midplane (at heights ±45 cm) could also be used for the detection system, but simulations showed that this would not produce any performance improvement.

Fig. 1 shows the port arrangement in the midplane and Fig. 2 the corresponding graphic output of the simulation code for a port angle separation α of 45^{o}, with the maximum possible injector tilt angle θ of $+11.25^{o}$ in positive (definition!) direction. 20 LOS are shown which cover the entire plasma cross-section. The positioning of these LOS in the code is variable.

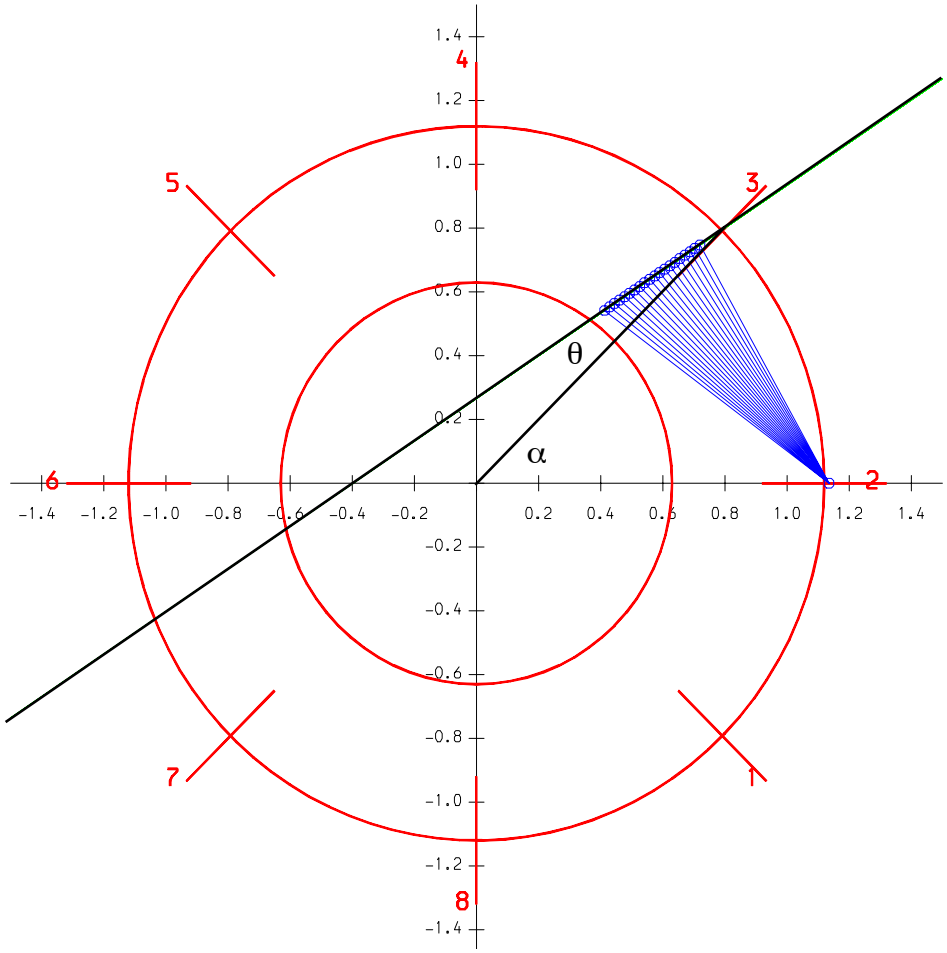

FIGURE 2. Layout projected on median plane. The 20 observation points on the beam line determine the LOS fan. The angle α between beam and observation port is 45^{o} and the injector angle θ is 11.25^{o}. The two circles indicate the vessel walls at R=0.62m and R=1.12m. The plasma center is at R=0.875m.

Since the second harmonic gyrotron launchers in TCV are placed in the midplane and 40 cm above, most plasmas are centered typically 20 cm above the midplane. For such plasmas a MSE set-up in the midplane would not be able to observe the plasma center and hence would probably not be able to distinguish plasmas with normal and reversed shear, constituting a significant drawback. This problem could be solved with a vertical beam injector through the plasma center. A new injector would have to be installed either above or below the machine. As will be shown, the results for these two options are comparable, as long as the larger distance from below has neither a significant effect on beam absorption nor beam divergence. Technically the installation of an NPI above the machine would be rather challenging to achieve, since no platform is available to support the injector.

Below the machine space is rather limited, but a pre-design study showed that placing the injector in this configuration would be possible.

3.0 The simulation code

Quantitative results have been obtained by using the MSE simulation code PERF [7] developed at JET. It simulates the spectrum and the intensities of the harmonics of the polarimeter output from which the expected measurement error in the polarization angle is obtained. In the code the following assumptions are made:

- The H_α or D_α emission only is considered,
- A simple elliptical equilibrium is assumed,
- The beam attenuation by protons and carbon is considered, assuming a fixed Z_{eff},
- The calculations are only done for the linear Stark regime, which is well satisfied,
- The Zeeman splitting is ignored.

3.1 Code algorithm

- A beamline is defined and along it, inside the plasma, a number (typically 20) of equidistant observation points.
- From a fixed observation port a fan of observation vectors are drawn towards these observation points.
- For each beam / observation vector intersection the B vector is calculated, based on the central B field, the elongation and an assumed q-profile.
- The beam density and the Doppler shift along the viewing line are then obtained.
- The E vector and its projections on the H and V directions of the LOS are calculated.
- The Stark spectrum (for all beam components), resolved in the H and V directions is computed.
- The total polarization resolved spectrum is then obtained, assuming gaussian broadening due to beam divergence and energy spread.
- The code has been modified to include the contribution of bremsstrahlung emitted by the plasma, but no other contribution to background radiation (edge H_α , C-X, CII lines) has been considered. The position of CII lines is shown in the output spectra, but not included in the calculation.
- From the spectra the measured flux at the polarimeter harmonics is computed from which the projected pitch angle γ and the Poisson uncertainties are obtained.
- The spatial resolution is obtained from the beam width and intersection geometry.

The code reads an input parameter file which has been adapted to TCV conditions. JET-specific parameters which were hard-wired into the code (geometry, beam parameters) have also been modified. Since the code uses JET-specific physics and graphics packages

all simulations were done remotely on JET computers and the results transferred to CRPP for data analysis, printing and plotting.

The output of the program consists of:

- several alphanumeric result files
- a postscript file with plots illustrating the geometry, assumed input density and q profiles, spectra for all LOS and the predicted polarization angles as function of distance along the beam, with error bars for both intensity and space resolution.

4.0 Results

4.1 General observations

The measurement precision depends in an obvious way on certain parameters. In particular, the error is inversely proportional to the square root of:

- the diagnostic sensitivity
- the beam power
- the integration time

The diagnostic sensitivity which is treated as a fixed input parameter, includes all elements of the detection system, including the beam transport system (lenses, fibres etc.). We used systematically the standard value for JET conditions of 3.5×10^{-11} counts/photon·m^{-2}. This value is based on the assumption of an étendue of 1×10^{-7} str·m^2, 8.8% overall transmission and 10% quantum efficiency of the photomultiplier. Small improvements of the latter two factors are perhaps possible, but only the étendue could potentially raise this value by a significant amount. The étendue of the MSE system on Asdex-U is reported to be 2.4×10^{-6} [8], hence 24 times larger than at JET. Assuming that light is collected from a circle of r = 2cm (this corresponds to the typical spatial resolution obtained with the code) in TCV and that the distance to the light collecting lens is 80 cm, then the solid angle is $\Omega = 1.5 \times 10^{-4}$ str. The port geometry in its present state would not allow a lens larger than 4 cm in diameter, resulting in a collection area of 10^{-3} m^{-2}. The étendue (1.5×10^{-7}) is then roughly comparable (50% larger) with the one at JET. If the CSX diagnostic was moved to a different location, larger (up to a factor of 2) lens/mirror arrangements could be considered. Order of magnitude improvements are not easily achieved, but several other factors involved in the overall sensitivity could be improved as well, so that the value used can be considered to be rather conservative.

In the optical transfer system the most important loss is due to the use of fibres. In particular the efficiency of coupling into and out of the fibres cannot be optimized beyond a certain value. To alleviate this situation, multiple fibres are generally used for each channel. On large machines like JET fibres have to be used because of the large distance to the detection system outside the biological shield. Fibres also allow to easily steer the light

and transport it exactly to wherever the detector is located. On TCV, at least for a vertical beam which also results in a vertical fan of LOSs, it might be possible to avoid fibres altogether. Space for a light-tight box encompassing the whole detection system can be found around the machine, but only a detailed design could provide a definitive answer.

As far as beam power is concerned, the main difference with the JET system is that there one of the heating beams with a power of 1 MW is used for the MSE diagnostic, whereas the existing NPI at TCV provides only 65 kW. The difference of a factor of 16 results in a difference in measurement precision of 4.

A series of simulation runs has further shown that the predicted measurement error is

- weakly dependent on the beam voltage and on n_e,
- and roughly proportional to B_0^{-x} , with $1.5<x<3$ for most of the studies reported here.

The last point indicates that high field conditions are much more favorable.

4.2 Typical scenarios

We have studied the following typical scenarios:

4.2.1 Normal shear

n_e: $2 \cdot 10^{19} < n_e < 1 \cdot 10^{20}$

B_T: $0.8T < B_T < 1.54T$ (typ. 1.43T)

κ: $1 < \kappa < 2.8$

Profiles:

- A quadratic n_e profile was chosen with $n_e^{edge} = 1 \cdot 10^{18}$
- for q we used a generic profile for circular machines with large aspect ratio [9]:

$$q = C\,(\nu + 1)\,\rho^2 / (1 - (1-\rho^2)^{\nu+1})\ ;$$ with $\nu = 2$ and $C=0.9$ this gives $q_o = 0.9$;

$q_{edge}=2.7$

4.2.2 Normal shear with high edge q

As 4.2.1, but $q_{edge} = 7$

4.2.3 Reversed shear

B_T: 1.43T

κ: $1.6 < \kappa < 2.4$

n_e: $1 \cdot 10^{19} < n_e < 3 \cdot 10^{19}$

q profile:

q_o: 2

q_{min}: 1 @ $\rho = 0.25$

q_{edge}: 8

A 6-order polynomial was used to provide a profile with these features.

4.3 Signal to noise ratio considerations

Based on the injector power reduced by plasma absorption, the Lorentz field at the point of observation, the Stark emission for the assumed plasma parameters and all the geometrical factors involved, the spectrally resolved intensity incident on the detection system is calculated by the code. For TCV conditions it is typically 10^{16} photons m^{-2} s^{-1} or $3x10^{-3}$ $Jm^{-2}s^{-1}$ per $\Delta\lambda$=0.03nm, the fixed "pixelwidth" of the code. With the assumptions made about the detection system described above, this corresponds to about 40 000 photons for the main polarization direction and to between 100 and 3000 photons for the other polarization. The measurement precision depends on photon statistics and the code predicts typically between a few and up to 10% error for the "measured" q-values. This is obtained under the assumption that no background radiation is superimposed on the signal at the entrance of the detection system.

The most important source of undesirable background radiation is line radiation due to impurities or unshifted H_α. The intensity level cannot be estimated easily since it depends critically on the measurement geometry. Fortunately these are features of narrow spectral width which can be avoided by a judicious choice of the Stark line used for the measurement and the measurement geometry. In particular at the lower densities which are interesting for EC heating and current drive studies, a background of molecular lines may also be present [10].

Fig. 3 shows a measured emission spectrum in the vicinity of the H_α line in the presence of a typical plasma, but without particle beam. The H_α line at 656.28 nm is clearly visible and also the C^{II} lines at the right of this feature. It shows that above 659nm and below 654nm no line radiation rising above the noise level is observed. A calibration indicated that this background noise corresponds to $1.2x10^{14}$ photons m^{-2} s^{-1}per pixel width. The signal to noise ratio at the input to the detection system is therefore of the order of 1%. Note that this ratio is obtained from reliable parameters. In particular the somewhat uncertain "diagnostic sensitivity" is irrelevant here, because the S/N comparison is done in front of the detector.

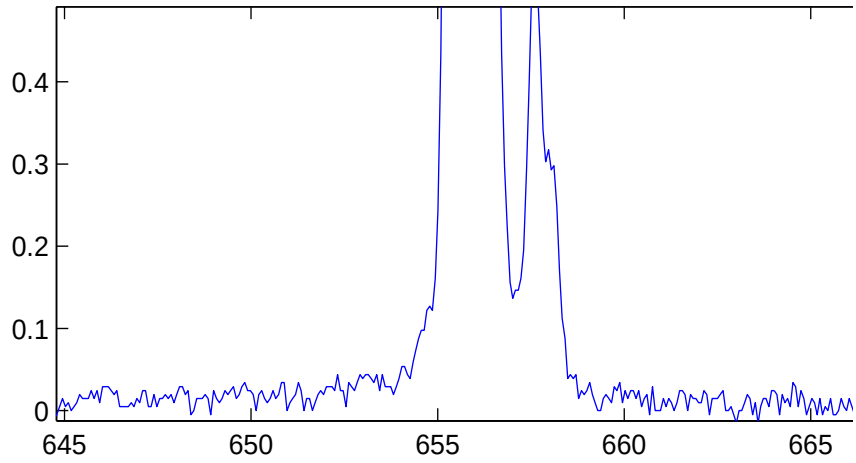

FIGURE 3. Measured background signal in the spectral region of interest in arbitrary units vs. wavelength in nm (courtesy I. Condrea)

In the absence of line radiation the most likely dominant source of this background radiation is bremsstrahlung radiation. Its intensity B_{brems} can be obtained from

(EQ 1)

$$B_{brems} = \frac{9.5 \times 10^{-20} \Delta\lambda}{4\pi\lambda} \int_{dl} \frac{\overline{g_{ff}} n_e^2 Z_{eff}}{T_e^{1/2} \exp(12400/T_e\lambda)} dl$$

with n_e in m^{-3} and T_e in eV. B_{brems} is in photons/(s m^2 sr).

A rough estimate for typical TCV conditions can be obtained with the following assumptions: λ=656nm and $\Delta\lambda$=0.03nm (the pixel width). Instead of profiles we take fixed average plasma parameters over a propagation distance of 0.8m, namely n_e=3 10^{19} m^{-3}, Z_{eff}=2.5, T_e=1000eV. g_{eff} and the value of exp are taken as 1. This gives B_{brems}=2 10^{13} photons m^{-2} s^{-1}, hence about 0.2% of the signal. This is 5 times lower than the measured background radiation. However, it would be premature to conclude that the measured background is composed of other contributions than bremsstrahlung radiation, because of the coarse assumptions made and the fact that the plasma parameters for the measured spectrum are not precisely known. In fact, we assume that bremsstrahlung is indeed the dominant background radiation and included its effect in the simulation code.

4.4 Optimization procedure

For a plasma centered in the mid-plane and a beam geometry according to Fig. 2 with the assumed q-profile and the centrally peaked density distribution shown in Fig. 4, the code predicts the measured polarization angle profile displayed in Fig. 5.

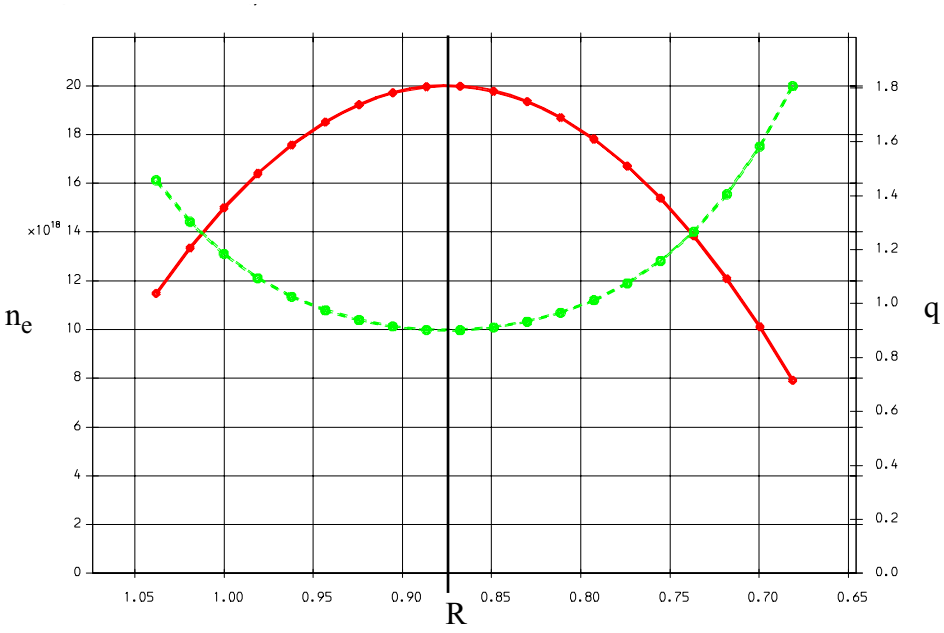

FIGURE 4. The solid line shows the assumed density profile and the broken line the q-profile for a case of normal shear with q=0.9 in the center and q=2.7 at the edge. The low field side is on the right in all plots of this type and the plasma center marked with a solid line at R=0.875m.

The error bars shown suggests that the accuracy for this (normal shear) case is reasonable for all LOS. However, if the MSE is used to determine the q-profile from the pitch angle measurements, the true question is with what precision the q-profile can be measured. This is the inverse problem of what the code has been designed to handle and adapting it correspondingly would require a major re-write. For this reason the following simplified procedure was adopted:

We claim that all values of q resulting in a "measured" polarization angle γ_m inside the polarization angle error bar are experimentally indistinguishable. The code is therefore run repeatedly with a range of q-values centered around the fixed q of each spatial point. All q-values resulting in a γ_m within the error bars of the simulation of the unmodified q-profile are considered to be indistinguishable. If γ_m for $q(1+N_1\%)$ is inside and for $q(1+N_2\%)$ is outside the error bar, we conclude that q can be measured with an accuracy of between N_1 and N_2 percent. The value assigned is then $(N_1+N_2)/2$ percent. An accuracy of 8.5% in q should be interpreted as meaning that q can probably be measured with between 8 and 9% accuracy. The discrete one percent steps could be refined by interpolation, but in the context of this study this was not considered to be essential. Note, however, that asymmetric error bars are usually obtained with this procedure and two values are therefore listed in the tables.

Applied to the case discussed it follows that only for the 7 innermost (R<0.875m) points q can be determined with an accuracy below 10% (±7% for most of them). Visual inspection of Fig. 5 would not lead to this conclusion, because the precision of γ_m of the outer points does not seem to be noticeably worse.

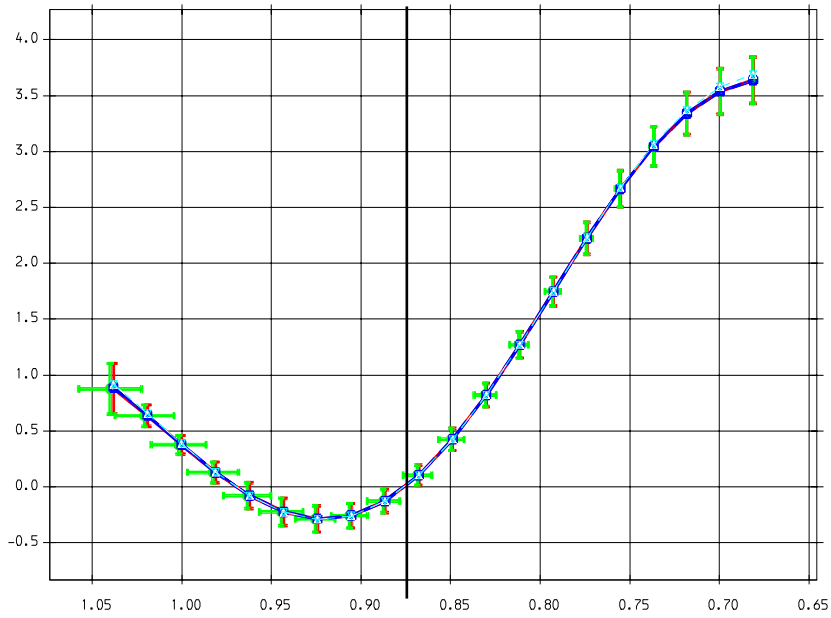

FIGURE 5. Calculated and "measured" pitch angle with error bars for the pitch angle and spatial position for the case of a normal shear q-profile. The angle between the beam and detection ports is 45^{o} and the injector angle $+11.25^{o}$ as Fig. 2. Note that in all plots obtained with the code the high field side is on the right with the plasma center at 0.875 m.

Fortunately a higher space resolution is predicted where the γ_m precision is better. Nevertheless, with a q-profile measurable on the inside only, this is not a case rendering useful results which can only be obtained by careful optimization of the whole setup. We will now describe in detail how this optimization is achieved. Beforehand we would like to mention that the inclusion of the measured background increases the error from 7 to 8%, whereas the bremsstrahlung effect does not noticeably change the results in this particular case.

A first optimization step involves the geometry. Larger angles between beam and observation ports offer higher Doppler shifts and projection factors at the expense of spatial resolution. The term "spatial resolution" needs to be defined. It does not describe the aiming accuracy of the beam and LOSs, both of which can be made quite precise with a careful alignment procedure. It rather defines the uncertainty concerning the distance along the LOS over which light is collected from because of the finite width of the particle beam, leading to a smearing out of the measured pitch angle.

A further optimization step concerns the placement of the spectral channel. It must be outside the region where line radiation is observed and hence either above 659nm or below 654nm, see Fig. 3. Furthermore it should be placed on top of an intense Stark line, but one which is sufficiently separated from other lines, in particular those with different polarization. It is in fact found that the purity of the polarization is more important than the spectral intensity within the channel. Hence the channel is normally placed on the Stark lines with the largest shift, because these do usually not or only weakly overlap with other lines.

The code produces a spectrum of the type shown in Fig. 6 for each LOS. The positions of the individual Stark lines are marked with vertical bars, in positive or negative direction, depending on polarization. The resulting polarization fraction is indicated by a dashed line. These plots are used as guidelines for the placement of the channel and the selection of the channel width. However, the information they provide is not sufficient to predict the result and full simulation runs have to be done for each case studied.

In the code the channel center is expressed with respect to a particular Stark line and the width is given in terms of Stark line separation. In this way filter center and width automatically follow the Doppler shift variation, although the two respective parameters in the code are fixed for all LOS. This means that all filters are assumed to be tuned to the same Stark line albeit at different frequencies. Since filters have to be individually tuned in any case, this constraint could be relaxed and for each LOS the Stark line with the best combination of intensity and polarization purity could be chosen. In general, however, it is found that the optimum selection of the filter characteristics for one LOS is also good for the other ones.

4.5 Optimization for a normal shear scenario

For a density and q-profile as described in 4.2.1 and a geometry with port distance of 45^o and injection angle -11.5^o (injector tilted in the direction opposite to the one shown in Fig. 2), the "measured" polarization angle γ_m with error bars and the space resolution are shown in Fig. 7 (B_o=1.43T, τ=0.01sec,κ=1.5). The fan of LOSs is displaced further out with respect to Fig. 2. The Stark lines are on the low wavelength side and the filters have been placed on the Stark line farthest from the H_α line. Fig 6 illustrates the situation. In fact, it shows the spectrum for the LOS aiming at the observation point at R=1.03 m. The polarization is well defined for this spectral position, but the intensity is higher at other wavelength. However, as already discussed, polarizational purity is more important than intensity. For the particular LOS shown, the filter is centered at a wavelength of 3.6 nm below the H_α line. For the outermost LOS this value is 3.95 nm and for the innermost 1.2 nm. Comparison with Fig. 3 shows that for the 5 innermost points interference from the broadened unshifted H_α background cannot be excluded.

Table I shows the radius R of the sample points, the lower and upper bounds of the precision of q and the space resolution. The value of q at the outside up to almost the center can be determined with typically ±6% precision with a space resolution around ±2 cm, whereas the accuracy of q is around 10% on the inside. In principle this shows that a pitch angle measurement is possible over the whole plasma cross-section. However, as mentioned above, the background noise might preclude a measurement at the 5 innermost points.

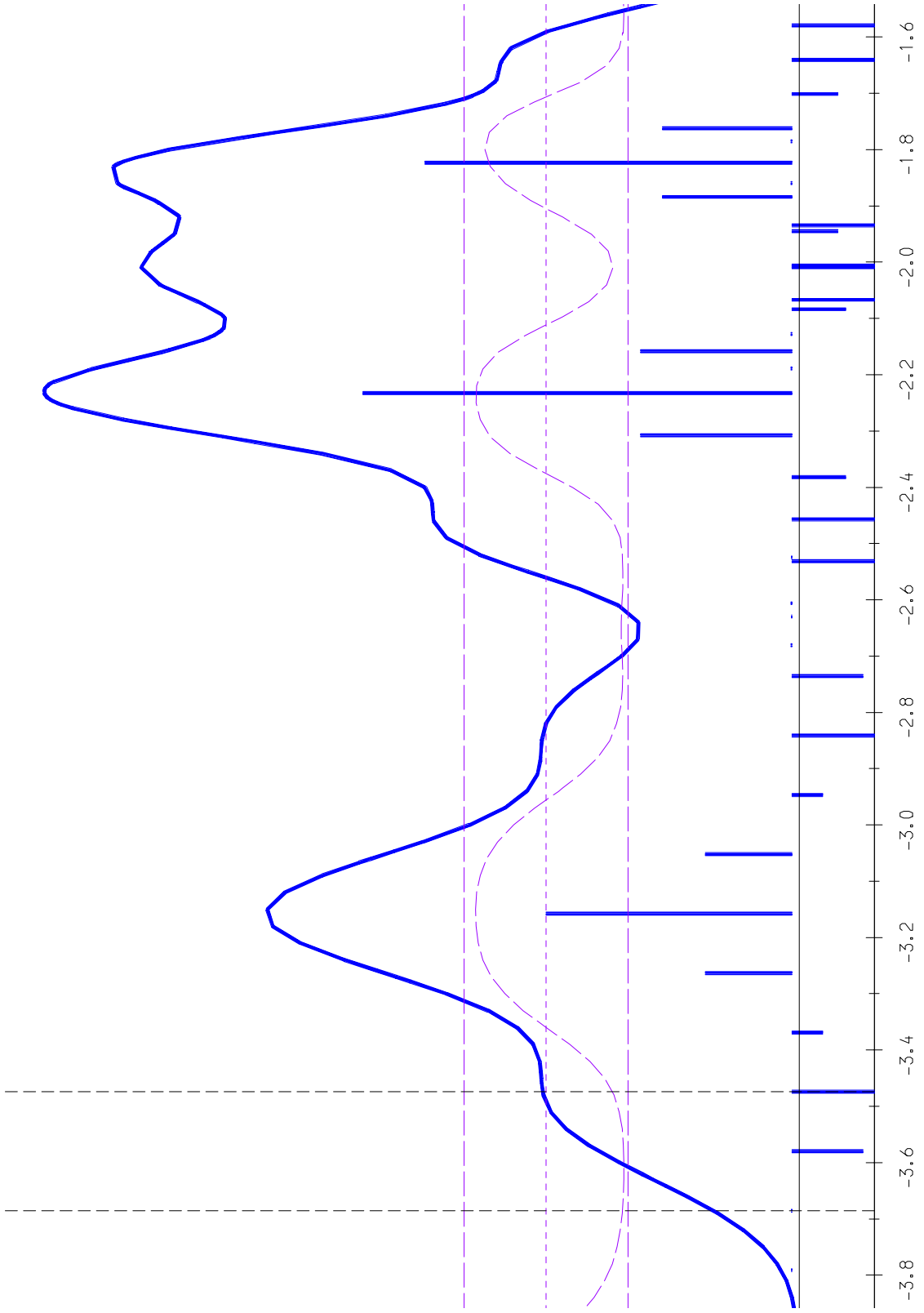

FIGURE 6. Emission spectrum for a particular LOS. The filter placement and width are marked by dashed vertical lines. Individual Stark lines are marked and also the polarization fraction. For details see text. The wavelength offset from H_α is in nm

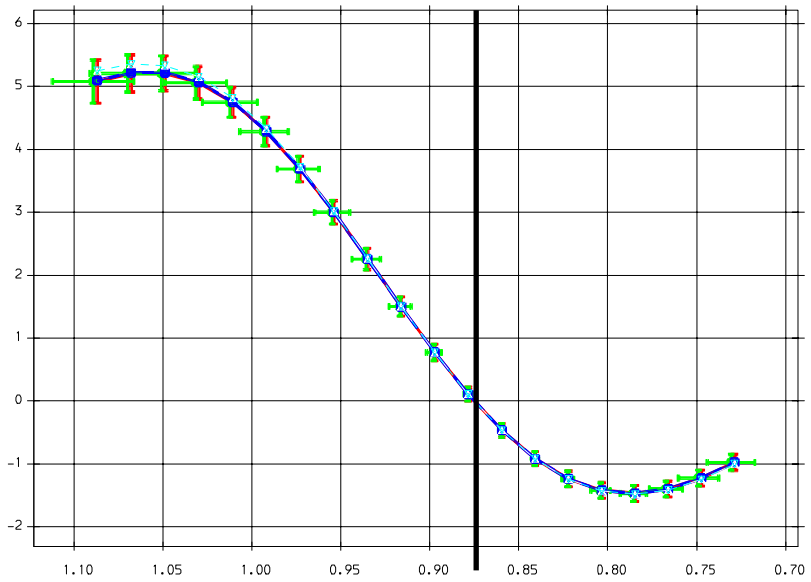

FIGURE 7. Simulated pitch angle measurement with error bars for the pitch angle and spatial position for the case of a normal shear q-profile. The angle between the beam and detection port is 45^0 and the injector angle -11.25^0. High field side on te right with plasma center at 0.875m.

The space resolution obtained with the code is based only on the fact that along the LOS light is collected from different parts inside the particle beam, but does not take into account the finite solid acceptance angle. In the discussion of the measurement sensitivity earlier on it was assumed that light is typically collected from a circle of 2 cm radius around the observation point. The true spatial accuracy can therefore not drop below ±2 cm for this acceptance angle. In order to profit from the calculated space resolution values below ±2 cm in table I the solid angle would have to be reduced, resulting in an increased uncertainty of the measured q. Hence a compromise has to be found between measurement precision and space resolution, depending on the ultimate use made of the data.

The pitch angle right in the center is zero, independent of q and hence q_o cannot be determined in this way. However, it can easily be shown that there is a simple relationship between the slope of the γ_m vs. position R curve and q_o at the central point. It is shown in Fig. 8. Since γ_m is zero in the center, the slope is proportional to the γ_m value at one of the neighboring points, to a good approximation. In fact, it is this value which is shown in Fig. 8, because experimentally this is how it would be done. The precision of q_o is determined by the error bar of γ_m at this neighboring point, because γ_m in the center is known to be zero independent of what the measurement indicates (which is only zero within the measurement precision). Of course, it is assumed here that this particular LOS is indeed aimed at the plasma center. This has to be confirmed independently. The procedure gives a q between 0.76 and 1.07 and thus the upper and lower bounds shown in the table for the central point (point #12).

TABLE 1. Expected positional and q accuracy for the conditions shown in Fig. 7. The value in the center (R=0.875m) has been obtained from the pitch angle slope (see text).

point #	R	lower bound (%)	upper q bound (%)	spatial q accuracy (cm)
1	1.087	-6.5	7.5	±2.3
2	1.068	-5.5	6.5	±2.1
3	1.049	-5.5	5.5	±1.9
4	1.030	-4.5	5.5	±1.7
5	1.011	-4.5	5.5	±1.6
6	0.992	-5.5	5.5	±1.4
7	0.973	-5.5	5.5	±1.2
8	0.954	-5.5	6.5	±1.0
9	0.935	-6.5	8.5	±0.8
10	0.916	-9.5	11.5	±0.6
11	0.897	outside 15	outside 15	±0.4
12	**0.878**	**-8.4**	**19.**	**±0.2**
13	0.860	outside 15	outside 15	±0.04
14	0.841	14.5	-10.5	±0.15
15	0.822	11.5	-9.5	±0.3
16	0.803	9.5	-7.5	±0.5
17	0.785	9.5	-7.5	±0.7
18	0.766	9.5	-8.5	±0.9
19	0.747	11.5	-9.5	±1.1
20	0.729	>15; <-15	>15; <-15	±1.3

Next a case has been investigated where the beam and diagnostic ports are 3 ports apart, that means forming an angle of 67.5^o. With an injector angle of +11.5^o no useful results are obtained, whereas with -11.5^o the measurement precision of q is very good, but the spatial resolution is worse than before. It is found that for this case the Stark lines of the different beam components are well separated, so that the detection channel could be placed on the π line on either side of the main σ line. The results are almost identical and are displayed in table 2. The accuracy of q is around 4% for most of the points. The procedure outlined above could again be used to determine the accuracy of q in the center. The spatial resolution, however, is considerably worse, especially at the outside.

A reasonably good precision can be obtained if the 2 ports are in the same vertical plane, however, the spatial resolution is unacceptable in this case. It becomes better if in addition to being on different horizontal levels, the ports are also in different vertical planes. The more interesting case is with θ=+11.5^o. The maximum angle γ_m reached (~14^o) is almost twice as large as in all other cases discussed so far. Measurements on the high field side

look quite promising and (less accurate) results can also be expected on the low field side, except too close to the edge.

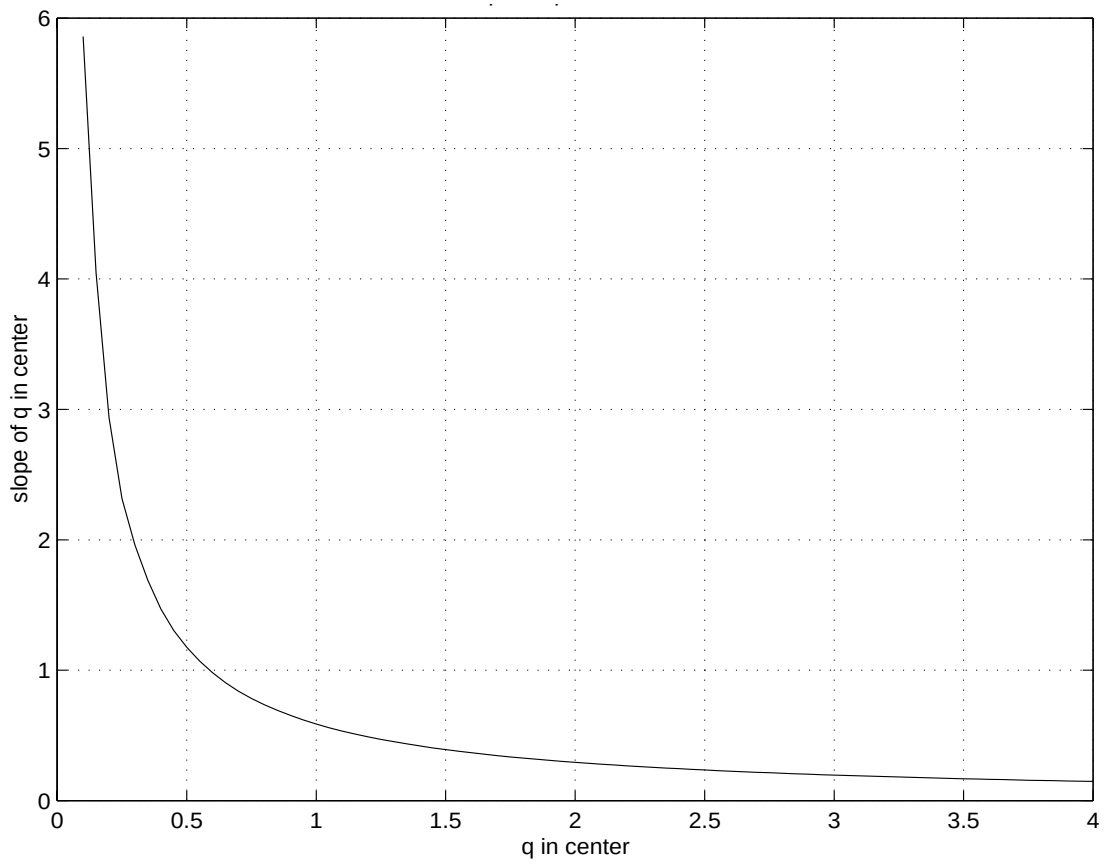

FIGURE 8. Slope of q versus q_o for central point. From the measurement precision of one of the neighboring points the slope precision is obtained and by means of this figure the expected accuracy of q in the center.

4.6 Normal shear with high edge q

We now investigate a situation similar to subsection 4.5, except that the edge q is higher ($q_{edge} = 7$). A promising geometry for this case is with both ports in the median plane, separated by 45^o and $\theta = -11.5^o$. The expected accuracy in q and the spatial resolution are shown in table 3.

Neither reducing the angle between ports to 22.5^o nor choosing the detection port above the median plane (for 22.5^o and 45^o) presents any advantage, as runs which are not shown here have demonstrated. However, separating beam and detection ports by 3 horizontal ports (angle 67.5^o) gives even better results as far as q is concerned, but – of course – with reduced spatial resolution. This is shown in table 4.

TABLE 2. Expected accuracy for an angle of 67.5^o between beam and diagnostic port and θ= -11.5^o. For case 1 the detector channel is placed on the π line on the high wavelength side of the main σ line and for case 2 on the low wavelength side. Point #12 is close to the center @ 0.875m.

point #	R	spatial accuracy (cm)	lower q bound case 1	upper q bound case 1	lower q bound case 2	upper q bound case 2
1	1.0916	±4.3	-4.5%	5.5%	-4.5%	5.5%
2	1.0723	±4.2	-3.5%	4.5%	-4.5%	4.5%
3	1.0531	±4.0	-3.5%	3.5%	-3.5%	4.5%
4	1.0339	±3.8	-3.5%	3.5%	-3.5%	3.5%
5	1.0148	±3.7	-3.5%	3.5%	-3.5%	3.5%
6	0.9956	±3.5	-3.5%	3.5%	-3.5%	3.5%
7	0.9765	±3.4	-3.5%	3.5%	-3.5%	3.5%
8	0.9574	±3.2	-3.5%	4.5%	-3.5%	4.5%
9	0.9383	±3.1	-4.5%	4.5%	-4.5%	4.5%
10	0.9192	±2.9	-5.5%	5.5%	-5.5%	6.5%
11	0.9001	±2.7	-7.5%	9.5%	-7.5%	9.5%
12	**0.8811**	**±2.6**	**outside15**	**outside 15**	**outside 15**	**outside 15**
13	0.8621	±2.4	12.5%	-10.5%	11.5%	-9.5%
14	0.8431	±2.2	7.5%	-6.5%	6.5%	-5.5%
15	0.8242	±2.1	5.5%	-4.5%	5.5%	-4.5%
16	0.8052	±1.9	4.5%	-4.5%	4.5%	-4.5%
17	0.7864	±1.7	3.5%	-3.5%	4.5%	-3.5%
18	0.7675	±1.5	3.5%	-2.5%	4.5%	-3.5%
19	0.7487	±1.4	3.5%	-2.5%	4.5%	-3.5%
20	0.7299	±1.2	3.5%	-3.5%	4.5%	-3.5%

.

TABLE 3. Expected spatial and q accuracy for a normal shear scenario with high edge q. The ports form an angle of 45^o and $\theta = -11.5^o$. Point #12 is close to the center at 0.875 m.

Point #	R	spatial accuracy (cm)	lower q bound (%)	upper q bound (%)
1	1.0870	±2.3	outside 15	outside 15
2	1.0679	±2.1	-9.5	12.5
3	1.0489	±1.9	-8.5	10.5
4	1.0299	±1.7	-7.5	9.5
5	1.0109	±1.6	-7,5	8.5
6	0.9919	±1.4	-7.5	8.5
7	0.9729	±1.2	-6.5	7.5
8	0.9540	±1.0	-6.5	7.5
9	0.9350	±0.8	-7.5	9.5
10	0.9161	±0.6	-9.5	12.5
11	0.8972	±0.4	outside 15	outside 15
12	**0.8784**	**±0.2**	**outside 15**	**outside 15**
13	0.8595	±0.04	outside 15	outside 15
14	0.8407	±0.2	14.5	-11.5
15	0.8220	±0.3	12.5	-9.5
16	0.8032	±0.5	11.5	-9.5
17	0.7845	±0.7	12.5	-9.5
18	0.7659	±0.9	14.5	-11.5
19	0.7473	±1.1	outside 15	outside 15
20	0.7287	±1.3	outside 15	outside 15

TABLE 4. As table 6, but with a port angle of 67.5^{o}. Point #12 is close to the center at 0.875 m.

Point #	R	spatial accuracy (cm)	lower q bound (%)	upper q bound (%)
1	1.0870	±4.3	-9.5	11.5
2	1.0679	±4.2	-7.5	8.5
3	1.0489	±4.0	-6.5	7.5
4	1.0299	±3.8	-5.5	6.5
5	1.0109	±3.7	-5.5	5.5
6	0.9919	±3.5	-4.5	5.5
7	0.9729	±3.4	-4.5	4.5
8	0.9540	±3.2	-4.5	4.5
9	0.9350	±3.1	-4.5	5.5
10	0.9161	±2.9	-5.5	6.5
11	0.8972	±2.7	-8.5	9.5
12	**0.8784**	**±2.6**	**outside 15**	**outside 15**
13	0.8595	±2.4	12.5	-9.5
14	0.8407	±2.2	7.5	-6.5
15	0.8220	±2.1	5.5	-5.5
16	0.8032	±1.9	5.5	-4.5
17	0.7845	±1.7	5.5	-4.5
18	0.7659	±1.5	5.5	-4.5
19	0.7473	±1.4	5.5	-5.5
20	0.7287	±1.2	6.5	-5.5

4.7 Reversed shear

A reverse shear q-profile described by a 6 order polynomial has been constructed, such that it has the following properties:

- q = 2 at the center
- q = 1 at ρ = 0.25
- q = 8 at the edge (ρ=1)

These 3 conditions together with the fact that the slopes at ρ=0 and ρ=0.25 are zero (2 more conditions) define a 4th order polynomial. However, this results in an unrealistic profile with a local maximum close to the edge, rather than a monotonic increase of q towards the edge. Since in the simulation program the n_e and q profiles are described by polynomials, we chose a 6 order polynomial for q and used the 2 free parameters in order to get a profile of the desired shape. It is shown in Fig. 9.

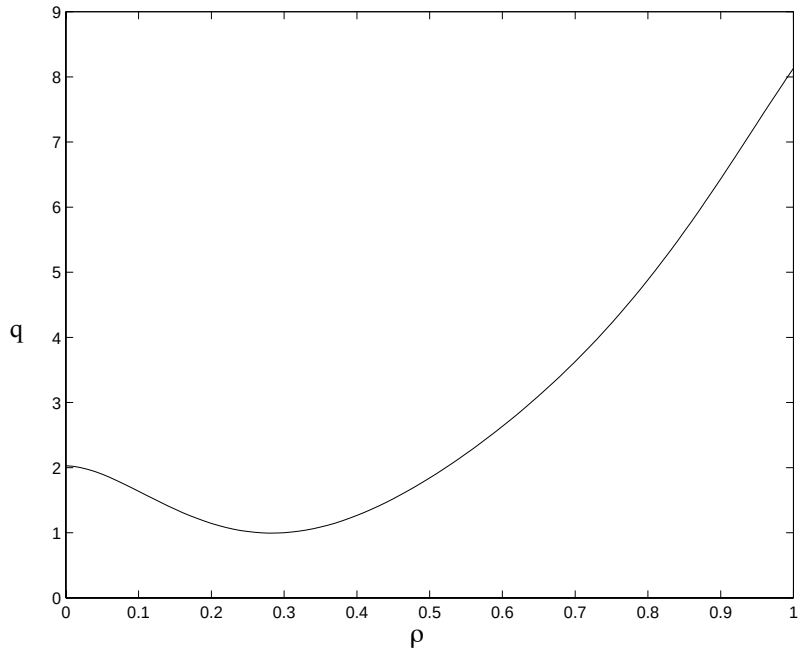

FIGURE 9. The q-profile for a synthetic reversed shear case described by a 6th order polynomial. q vs ρ is shown.

Similar to the results with normal shear it is found that only 2 geometries look promising: beam and observation port in the same horizontal plane and separated either by 45^o or 67.5^o. The angle of the injector should be -11.5^o which is different from Fig.2. The larger angle (67.5^o) gives better accuracy in q, but less precise space resolution, whereas for the angle of 45^o the opposite is true. We compare these two cases in table 5.

Finally we present a case with larger elongation: $\kappa = 2.4$ (instead of 1.5 as in all previous cases). In this case, and for the angle of 45^o with the better spatial resolution, the simulation indicates that q can be measured for all except the 3 points in the middle where q can be obtained from the slope. The spatial resolution is identical to the case 1 above and q and the expected measurement precision are shown in graphical form in Fig. 10.

4.8 Plasma centre above median plane

The conditions on TCV are such that during high power ECR/ECCD plasmas with centres of up to 21 cm above the median plane are preferred, with typical values of 10 and 21 cm. No ports for the beam injector exist at these levels: the next horizontal plane with ports is 45 cm above the median plane, which is not suitable.

While it is likely that a measurement with an LOS fan below the plasma centre is feasible, the important question here is, whether it is still possible to distinguish an inversed shear plasma from a normal one. At the height of 21 cm this is no longer the case, whereas at 10 cm it is possible for high elongation ($\kappa = 2.4$). The density and q-profiles then look as

shown in Fig. 11. The error bars are those obtained from the simulation. Their size indicates that a reverse shear case can indeed be distinguished from a normal one for these conditions. The accuracy in q and spatial resolution are good, as shown in table 6 for port angles of 45^o and 67.5^o.

TABLE 5. Comparison of negative shear simulations with angles of 45^o (case 1) and 67.5^o (case 2) between beam and observation ports. The injector angle is -11.5^o in both cases. Point #12 is close to the center at 0.875 m

Point #	R	spatial accuracy case 1 (cm)	lower q bound case 1 (%)	upper q bound case 1 (%)	spatial accuracy case 2 (cm)	lower q bound case 2 (%)	upper q bound case 2 (%)
1	1.0870	±2.3	outside 15	outside 15	±4.3	-10.5	12.5
2	1.0679	±2.1	-10.5	12.5	±4.2	-7.5	9.5
3	1.0489	±1.9	-8.5	10.5	±4.0	-6.5	7.5
4	1.0299	±1.7	-7.5	9.5	±3.8	-5.5	6.5
5	1.0109	±1.6	-6.5	8.5	±3.7	-5.5	5.5
6	0.9919	±1.4	-6.5	7.5	±3.5	-4.5	4.5
7	0.9729	±1.2	-5.5	6.5	±3.4	-4.5	4.5
8	0.9540	±1.0	-5.5	6.5	±3.2	-3.5	4.5
9	0.9350	±0.8	-7.5	8.5	±3.1	-4.5	5.5
10	0.9161	±0.6	outside 15	outside 15	±2.9	-6.5	7.5
11	0.8972	±0.4	outside 15	outside 15	±2.7	outside 15	outside 15
12	**0.8784**	**±0.2**	**outside 15**	**outside 15**	**±2.6**	**outside 15**	**outside 15**
13	0.8595	±0.04	outside 15	outside 15	±2.4	outside 15	outside 15
14	0.8407	±0.2	outside 15	outside 15	±2.2	9.5	-7.5
15	0.8220	±0.3	12.5	-10.5	±2.1	5.5	-5.5
16	0.8032	±0.5	9.5	-8.5	±1.9	4.5	-4.5
17	0.7845	±0.7	10.5	-8.5	±1.7	4.5	-4.5
18	0.7659	±0.9	13.5	-10.5	±1.5	4.5	-4.5
19	0.7473	±1.1	outside 15	outside 15	±1.4	5.5	-4.5
20	0.7287	±1.3	outside 15	outside 15	±1.2	6.5	-5.5

TABLE 6. Comparison of spatial and q accuracy for a plasma with centre 10 cm above median plane. The toroidal angle is 45 and 67.5^o. Point #12 is close to the center at 0.875m.

Point #	R	spatial accuracy (cm) $\theta=45^o$	lower q-bound (%) $\theta=45^o$	upper q-bound (%) $\theta=45^o$	spatial accuracy (cm) $\theta=67.5^o$	lower q-bound (%) $\theta=67.5^o$	upper q-bound (%) $\theta=67.5^o$
1	1.087	±2.3	-9.5	12.5	±4.3	-7.5	9.5
2	1.068	±2.1	-7.5	9.5	±4.2	-5.5	6.5

TABLE 6. Comparison of spatial and q accuracy for a plasma with centre 10 cm above median plane. The toroidal angle is 45 and 67.5^o. Point #12 is close to the center at 0.875m.

Point #	R	spatial accuracy (cm) θ=45^o	lower q-bound (%) θ=45^o	upper q-bound (%) θ=45^o	spatial accuracy (cm) θ=67.5^o	lower q-bound (%) θ=67.5^o	upper q-bound (%) θ=67.5^o
3	1.049	±1.9	-6.5	7.5	±4.0	-4.5	5.5
4	1.030	±1.7	-6.5	6.5	±3.8	-4.5	4.5
5	1.011	±1.6	-5.5	6.5	±3.7	-4.5	4.5
6	0.992	±1.4	-5.5	5.5	±3.5	-3.5	3.5
7	0.973	±1.2	-4.5	5.5	±3.4	-3.5	3.5
8	0.954	±1.0	-4.5	5.5	±3.2	-3.5	3.5
9	0.935	±0.8	-4.5	5.5	±3.0	-3.5	3.5
10	0.916	±0.6	-5.5	6.5	±2.9	-3.5	4.5
11	0.897	±0.4	-7.5	9.5	±2.7	-4.5	5.5
12	**0.878**	**±0.2**	**outside15**	**outside15**	**±2.6**	**outside15**	**outside15**
13	0.860	±0.04	13.5	-10.5	±2.4	6.5	-5.5
14	0.841	±0.15	8.5	-7.5	±2.3	4.5	-4.5
15	0.822	±0.3	6.5	-6.5	±2.1	3.5	-3.5
16	0.803	±0.5	6.5	-6.5	±1.9	3.5	-3.5
17	0.784	±0.7	7.5	-6.5	±1.7	3.5	-3.5
18	0.766	±0.9	9.5	-7.5	±1.5	4.5	-3.5
19	0.747	±1.1	12.5	-10.5	±1.4	4.5	-4.5
20	0.729	±1.3	outside 15	outside 15	±1.2	4.5	-4.5

5.0 Vertical injector

With a vertical beam line it would be possible to sample the plasma independently of its height above the median plane, provided the detection system can be placed appropriately. A preliminary study has shown that an injector could be installed below the machine. It would have to be an additional injector, contrary to all cases studied so far where it was assumed that the existing one [11] would be used. At the present stage this has to be considered as a somewhat exotic project and hence we used existing ports for the diagnostic system without concern for their availability.

An obvious choice would be a vertical beam through the plasma centre and a diagnostic port in the same plane defined by the beam and the machine centre. Indeed a measurement would be possible, but with error bars exceeding 10% for all points. The spatial resolution in radial direction in this case is given by the beam diameter and hence ±7.5 cm, with an accuracy in vertical direction exceeding ±10 cm for most points. Stark lines with different polarization properties overlap in this case so that no filter position can be found with clearly defined polarization.

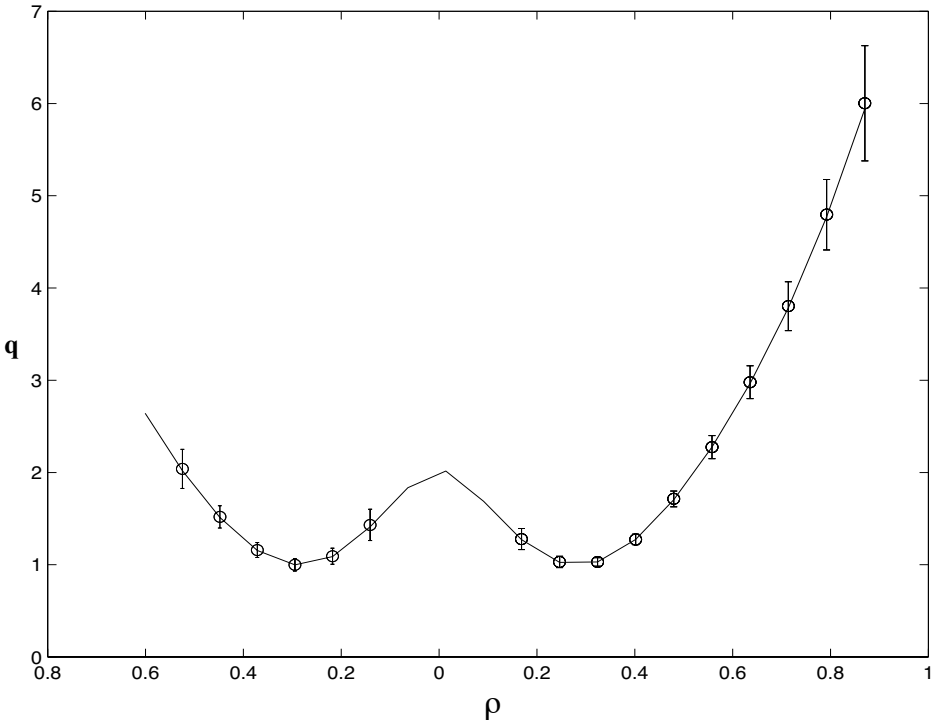

FIGURE 10. Expected precision of a q-measurement for κ=2.4, port angle = 45^o, θ=-11.5^o. The plot shows q vs ρ. For 4 points the error exceeds 15%

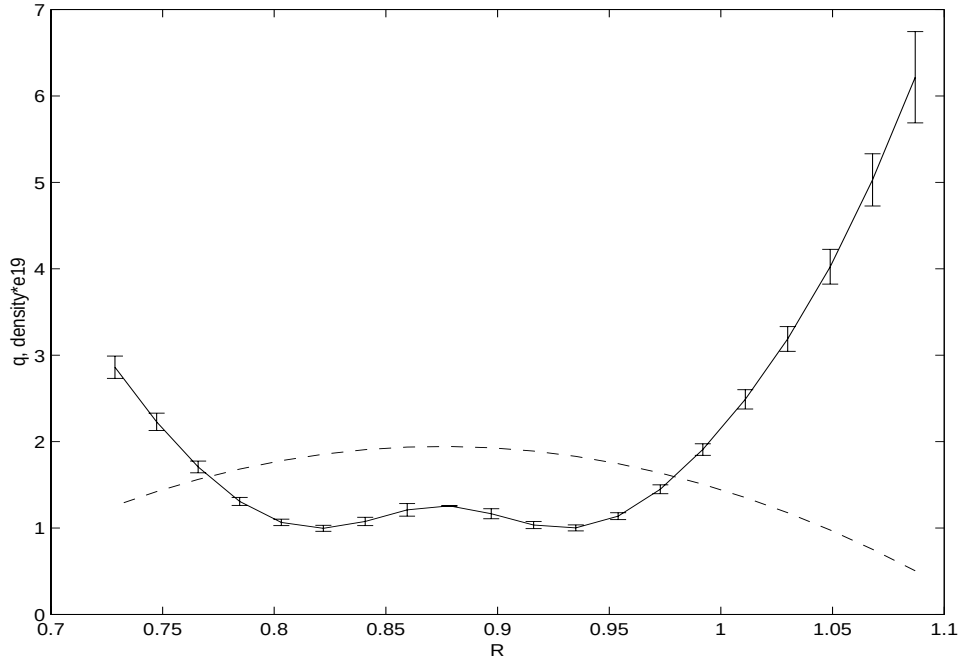

FIGURE 11. Density and q-profile in median plane for a plasma with κ = 2.4, 10 cm above the median plane. The error bars are obtained from the simulation.

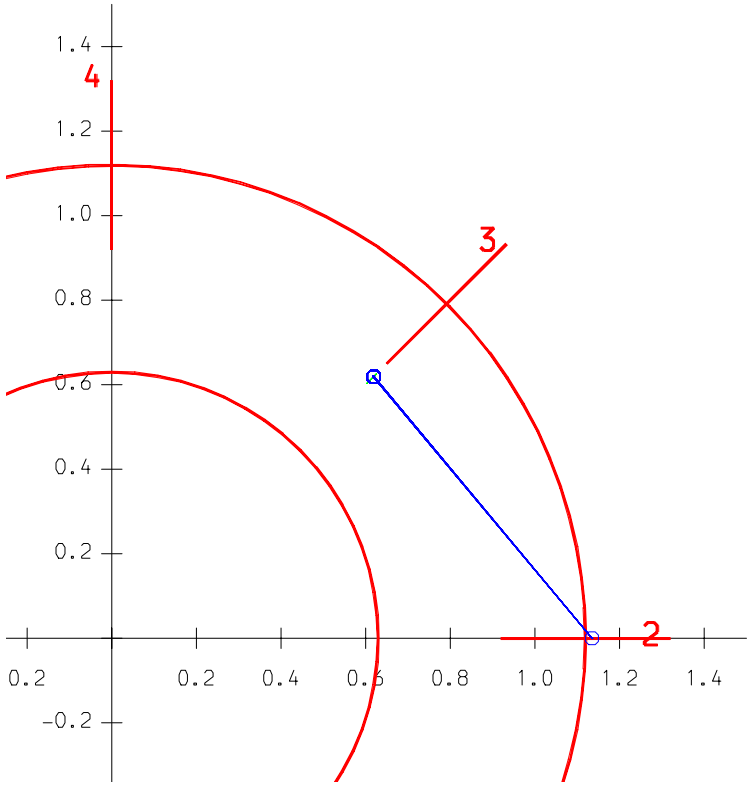

FIGURE 12. Geometrical arrangement for a vertical beam with the detection system toroidally separated by 45^{o}.

Displacing the diagnostic equipment in toroidal direction improves the situation. An almost ideal arrangement is found to be a separation of beam and detector by a toroidal angle of 45^{o}. This is not only a good compromise as far as the spatial accuracy is concerned, but since the LOS fan is almost tangential to the toroidal field, the precision of the pitch angle measurement is also very good. However, the diagnostic port has to be either above or below the midplane. In the midplane the spatial resolution is better, but the precision of γ_m is much worse.

The geometrical arrangement projected on the median plane is illustrated in Fig. 12. Obviously the vertical beam appears as point and the LOS fan as single line in this representation.

Fig. 13 shows the assumed density and q profiles and the measured polarization angle. Beam injection is from below the machine. The plasma with an elongation of 1.5 is centred 21 cm above the median plane and the observation points are at the heights between -16 and +21 cm and hence cover the lower part of the plasma cross-section. The diagnostic port is 45 cm below the median plane. As usual a measurement in and very close to the plasma center is not possible. This time γ_m is not zero for this point. In principle it can again be determined by the slope. However, in this case this does not produce a satisfact-

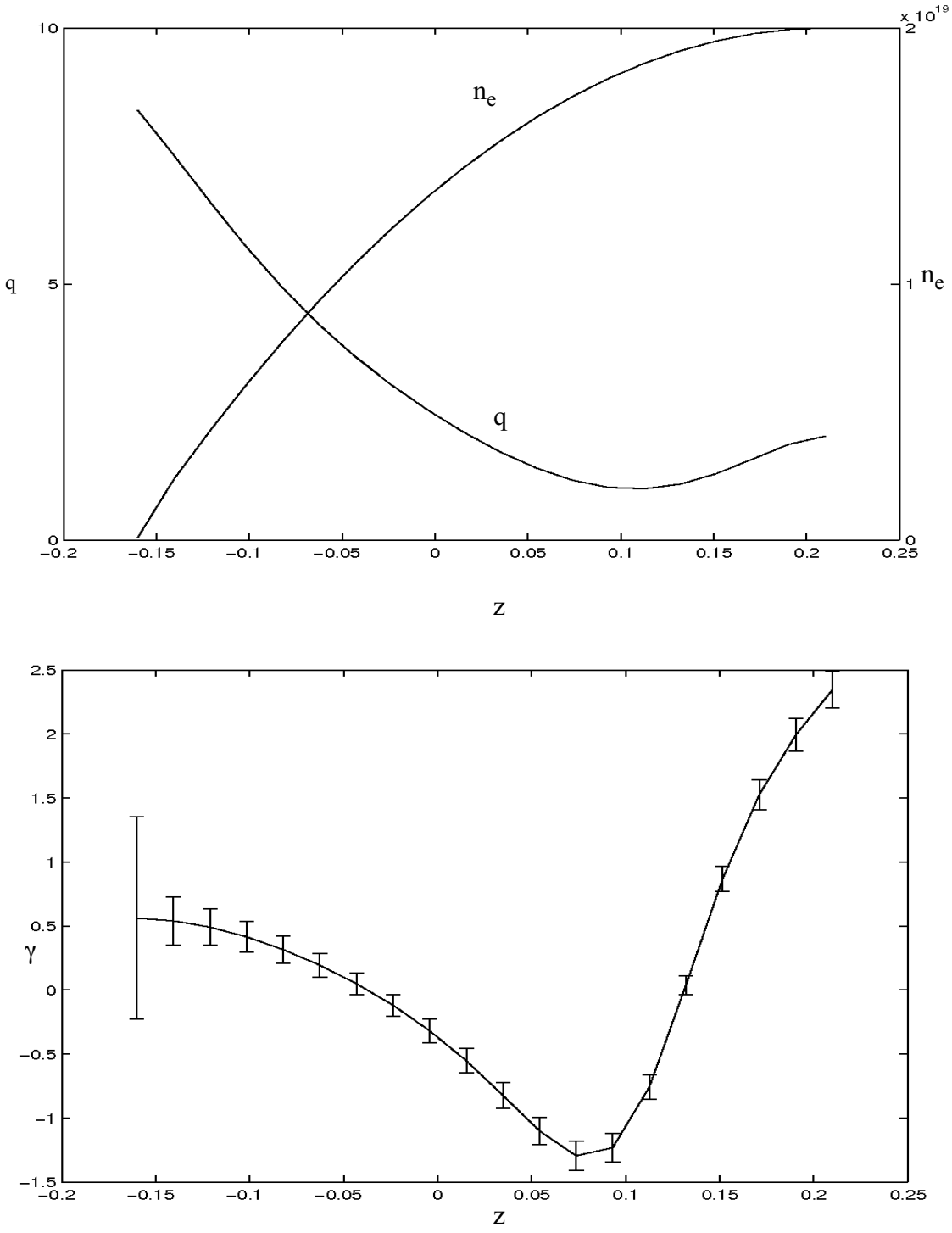

FIGURE 13. Vertical density and q-profile in upper part. Measured pitch angle in lower part. The plasma is 21 cm above the median plane and the detector 45 cm below this plane. The measurement covers heights from -16cm to 21cm. Injection is from below. The angle between injection and detection port is -45^{o}.

tory result.

In table 7 we show the results for the 2 cases of vertical beams with the detector displaced by 45^{o} in toroidal direction and either 45 cm below or above the midplane. In either case the beam is injected from below and the measurement points cover the region from the lower plasma edge to the center. For vertical beam calculations the code has been modi-

TABLE 7. Expected accuracy in q and z.for the case of a vertical beam. Spatial accuracy in R better than ±0.5 cm in all cases. Toroidal angle beam-diagnostic port -45^{o}. Plasma 21 cm above midplane. Case 1: detector 45cm above midplane, case 2: detector 45 cm below midplane

Point #	z (m)	spatial accuracy (cm) case 1	lower q-bound (%) case 1	upper q-bound (%) case 1	spatial accuracy (cm) case 2	lower q-bound (%) case 2	upper q-bound (%) case 2
1	-0.160	±5.7	outside15	outside15	±2.7	outside15	outside15
2	-0.141	±5.5	outside15	outside15	±2.9	outside15	outside15
3	-0.121	±5.3	-9.5	11.5	±3.1	14.5	-11.5
4	-0.102	±5.1	-7.5	8.5	±3.2	10.5	-8.5
5	-0.082	±5.0	-6.5	7.5	±3.4	8.5	-6.5
6	-0.063	±4.8	-5.5	5.5	±3.6	6.5	-5.5
7	-0.043	±4.6	-4.5	5.5	±3.8	4.5	-4.5
8	-0.024	±4.4	-3.5	4.5	±4.0	4.5	-3.5
9	-0.004	±4.2	-3.5	4.5	±4.1	4.5	-3.5
10	+0.015	±4.0	-4.5	4.5	±4.3	3.5	-3.5
11	+0.035	±3.9	-3.5	3.5	±4.5	3.5	-3.5
12	+0.054	±3.7	-3.5	3.5	±4.7	3.5	-3.5
13	+0.074	±3.5	-3.5	3.5	±4.9	3.5	-3.5
14	+0.093	±3.3	-4.5	4.5	±5.0	3.5	-3.5
15	+0.113	±3.1	-4.5	4.5	±5.2	3.5	-3.5
16	+0.132	±3.0	-5.5	6.5	±5.4	3.5	-3.5
17	+0.152	±2.8	-10.5	13.5	±5.6	7.5	-6.5
18	+0.171	±2.6	outside 15	outside 15	±5.8	outside15	outside15
19	+0.191	±2.4	outside 15	outside 15	±6.0	outside15	outside15
20	+0.210	±2.2	outside 15	outside 15	±6.1	outside15	outside15

fied in order to determine the spatial resolution in both R and z. In table 7 the spatial accuracy is given for the z-direction. For R it is better than ±0.5 cm in all cases.

With beam injection from above the distance from the plasma could be smaller. This only presents an advantage if either the absorption outside the plasma or the beam divergence is significant. In the code it is assumed that plasma absorption starts with the first observation point the beam encounters. This could be modified in order to include absorption in the region outside the plasma of interest (basically outside the last closed flux surface), but realistic beam absorption would better be based on measurements.

6.0 Conclusions

The MSE simulation code "perfd" has been an invaluable tool to investigate certain aspects of the feasibility of an MSE diagnostics on TCV. In particular, it allowed to determine which geometrical arrangements are most promising. Quite clearly this seems to be an arrangement with beam port and diagnostic port in the same horizontal plane and displaced by 2 or 3 ports, viz. angles of 45^o and 67.5^o respectively. In both cases the beam axis should be turned by an angle of 11.5^o with respect to the radial direction, towards the diagnostic port. In the first case the spatial resolution is better and in the second case the q measurement accuracy looks more promising. However, the differences are not so pronounced and other criteria could be invoked to favour one or the other option, for example the impact on other diagnostics.

However, a decision on whether to build such a system for TCV or not, should not be based on code results alone. In particular two aspects require special attention:

- Although background radiation effects have been included in the code, more detailed measurements are required to verify if background radiation – and in particular impurity lines – could pose a serious problem in the spectral regions of interest. Fig. 3 shows that at least on the low wavelength side there are no spectral lines or broadband background radiation of measurable intensity. More detailed studies are required for other cases. It is known, for example, that the H_α line gets very intense during ELMs.
- Although the detection sensitivity used in the code is based on a measurement done at JET, assuming that a similar set-up would be used, it was found at JET that longer integration times were required to get agreement between predictions and measurements. We propose a measurement of the signal to noise ratio for the 2 directions of polarization and for unpolarized radiation by using a modulated beam. By fitting the code results to these measurements a better estimate of the detection sensitivity could be obtained.

If it is found that the code predictions are optimistic, the integration time can still be used as an adjustable parameter up to some degree. In all simulations done the integration time was taken to be 10 ms. Values up to 50 or 100 ms could probably still be envisaged, but much beyond this the technique could no longer considered to be "time-resolved".

The main aim of such a diagnostic would be to provide valuable input to profile reconstruction codes (EFIT at JET or LIUQE at CRPP). At JET EFIT can be run with MSE data included or not and this allows to demonstrate what kind of improvement can really be obtained with an MSE diagnostic. The modification of LIUQE to include MSE data requires a significant amount of work and is probably not justified at this stage. It would, however, have to be done in case such a system would be implemented at TCV.

Geometries with vertical beam injection look quite promising. This would require a new injector with comparable – if not better – power than the present one. Because of the larger distance from the plasma the beam divergence should be equal or better than with the existing injector.

Apart from a detailed discussion concerning the potential of an MSE diagnostic with the predicted measurement quality for the scientific programme of TCV, financial and man power requirements will have to be considered.

Acknowledgment

This work was partly supported by the Fonds National Suisse de la Recherche Scientifique.

References

[1] F.M. Levinton et al., Phys. Rev. Lett. **63**, 2060 (1989)

[2] N.C. Hawkes et al., Rev. Sci. Instrum. **70**, 894 (1999)

[3] D. Wroblewski et al., Rev. Sci. Instrum. **63**, 5140 (1992)

[4] P. Lotte et al., 29th EPS CPPC, ECA **26B**, O-2.01 (2002)

[5] F.M. Levinton, Rev. Sci. Instrum. **70**, 810 (1999)

[6] J. Hobirk et al., Advanced Diagnostics for Magnetic and Inertial Fusion, Proc. of the International Conference on Advanced Diagnostics for Magnetic and Inertial Fusion, Sept. 3-7, Varenna, Italy, Kluwer Academic/Plenum Publishers, July 2002

[7] N.C. Hawkes, Design Study of a Motional Stark Effect Diagnostic for JET, report JET-R(96)10 (1997)

[8] R.C. Wolf et al., 24th EPS CFPP, ECA **21A**, 1509 (1997)

[9] John Wesson, Tokamaks, Clarendon Press, Oxford 1997, pg 114

[10] G. Sergienko et al., 26th EPS CCFPP, ECA Vol. **23J**, 725 (1999)

[11] J.Mlynar et al., Diagnostic Neutral Beam Injector at the TCV Tokamak, CRRP report, LRP 710/01, October 2001